Available online at www.sciencedirect.com
SCIENCE DIRECT®
Journal of Computational Physics 206 (2005) 277–301
JOURNAL OF COMPUTATIONAL PHYSICS
www.elsevier.com/locate/jcp

Capillary impregnation in a flexible slit: a finite element formulation

Srinath Madasu *

Department of Chemical Engineering, The Pennsylvania State University, University Park, PA 16802, USA

Received 7 July 2004; received in revised form 27 September 2004; accepted 24 October 2004
Available online 28 January 2005

Abstract

Dynamic wetting is an important phenomenon in many applications involving motion of liquid/vapor free surface on a solid surface. Capillary impregnation in a slit is one such important application. Modeling of this application is more challenging in a flexible slit than rigid slit since the solid deformation needs to be accounted in addition to tracking the contact line. Previously, a finite element model has been formulated for predicting dynamic wetting on flexible solids with upstream end of slot coater [S. Madasu, R.A. Cairncross, Effect of substrate flexibility on dynamic wetting: A finite element model, Comput. Methods Appl. Mech. Eng. 192 (2003) 2671–2702] as the prototype. This paper presents an application of that formulation in a moving reference frame for predicting the location of dynamic contact line for capillary flow inside a flexible slit. Arbitrary Lagrangian Eulerian (ALE) mesh motion is used to track the location of the contact line. Two singularities arise at the contact line: (i) in the solid domain due to liquid/vapor surface tension force acting as a line force and (ii) in the liquid domain due to the double-valued velocity. "Navier slip condition" and "Distributed line force condition" are used to relieve the singularities in the solid and liquid domains, respectively. The variation of dynamic contact line position with respect to various parameters such as pressure, contact angle, capillary number and elasticity number are presented for the finite element model and compared with an analytical model. The trends for the variation of length of penetration of liquid for rigid solid with inlet pressure, contact angle and capillary number compare qualitatively with the Washburn's equation (1).

MSC: 65N30; 76D45
Keywords: Dynamic wetting; Fluid–structural interactions; Capillary impregnation; Pseudosolid mesh motion; Arbitrary Lagrangian Eulerian mesh motion; Spine method of mesh motion; Finite element; Contact angle; Singularity; Capillarity; Flexible slit

* Tel.: +1 814 863 9543/215 868 0316; fax: +1 814 865 7846.
E-mail address: sum13@psu.edu.

0021-9991/$ - see front matter
doi:10.1016/j.jcp.2004.11.035

1. Introduction

Capillary impregnation of liquid in a slit is an important application of wetting [1,2] of solid. Wetting of the solid occurs at the intersection of solid/liquid, liquid/vapor and solid/vapor free surfaces, which is the *contact line*. The motion of contact line involves the movement of liquid/vapor free surface across the solid surface. Several researchers [3–5,9–12] in the past have studied the problem of motion of dynamic contact line in a rigid slit or tube solving for the velocity, pressure fields and liquid/vapor free surface shapes. Washburn [3] is one of the earliest researchers who studied the motion of liquids in small capillaries. He derived the simplified Eq. (1) for the velocity in a horizontal straight capillary tube attached at one end to a liquid column of height h and assuming very small capillary such that the Poiseuille flow assumption and radius of curvature being circular near the liquid/vapor meniscus are valid all the way until the meniscus:

$$U = \frac{\mathrm{d}l}{\mathrm{d}t} = \frac{\left[P_{\mathrm{A}} + g\rho h + \frac{2\sigma_{\mathrm{LV}}\cos\theta}{a}\right](a^2 + 4\varepsilon a)}{8\mu l}, \tag{1}$$

where U is the velocity of the liquid, l is the length of penetration, t is the time of penetration, P_{A} is the atmospheric pressure, g is the gravitational constant, ρ is the density of liquid, h is the height of the liquid column, a is the radius of the capillary, σ_{LV} is the liquid/vapor surface tension, μ is the viscosity of the liquid, ε is the slip coefficient and θ is the contact angle. Eq. (1) gives the relationship between the length of penetration and different parameters for rigid capillaries and hence, will be used for qualitative comparison of the results in this paper for rigid slits.

Several researchers have given numerical solutions [4,9–12] and theoretical solutions [4,5] of liquid/vapor free surface flow under both steady [4,5,9,10] and unsteady [11,12] flow conditions in a rigid capillary. Hansen and Toong [4] considered the steady motion of a viscous liquid in a tube to solve for the liquid/vapor free surface shape. They developed an approximate asymptotic outer solution for flow and also numerically solved the fluid motion along with interface shape to predict the liquid/vapor free surface shape. Their solution is valid at a distance 10^{-6}–10^{-5} cm from the intersection of the liquid/vapor free surface with the solid wall. Huh and Mason [5] modeled the steady movement of the liquid meniscus in a rigid capillary tube by developing an approximate analytical asymptotic solution. They obtained this solution valid for the entire flow region by matching the outer solution, which is valid away from the contact line and inner solution, which is valid near the contact line. They used slip to obtain the inner solution unlike Hansen and Toong, who only solved for the outer solution. They accounted for slip by considering two models, namely, Navier slip [6–8] over a slip length and free slip over a slip length and no slip thereafter. They calculated the correction factor for the length of penetration due to the curvature of the meniscus using their solution for dynamic contact angles close to 90°. Lowndes [9] carried out the numerical simulation using finite element method to study the meniscus shape for steady movement of fluid/vapor interface in a rigid capillary tube with change in capillary number. He used Navier slip condition to relieve the singularity. The meniscus profile is calculated by iterative scheme, where a profile was guessed and the Navier–Stokes equation along with continuity was solved except taking into account the normal stress balance condition at the meniscus and then the update for the meniscus profile was made by checking the normal stress balance condition. Tilton [10] modeled the steady motion of the interface between two viscous fluids in a rigid capillary tube using finite element method and presented the meniscus profile for various capillary numbers, contact angles and viscosity ratios. He used Navier slip condition to relieve the singularity. He concluded that at lower capillary numbers, viscous effects are unimportant and the interface shape is not deformed. As the capillary number is increased, the meniscus deformation increases.

Trutschel and Schellenberger [11] presented transient simulations of liquid–gas interface motion in capillaries for tubes and gaps using CFD code FIDAP, which is based on finite element method. They solved the transient fluid mechanics equations along with the free surface conditions for capillary rise and obtained

good comparison with the experimental values. Powell and Savage [12] solved for the transient free surface flow of capillary motion between horizontal rigid plates using Lagrangian finite element formulation. They removed the liquid stress singularity by using linear slip velocity distribution and used Tanner's law to relate the contact angle and velocity at the contact line.

All the studies that were done on dynamic wetting phenomena of capillary impregnation in the literature so far are on rigid tubes and slits. This paper presents a numerical finite element model for *capillary impregnation in a flexible slit*. Finite element formulation developed by Madasu and Cairncross [13] for dynamic wetting on flexible substrates will be used for modeling *capillary* impregnation in a flexible slit. This formulation has important modeling applications such as flow through porous media, studying flexible roll coating process, flexible blade coating process, etc. The study of capillary impregnation flow of liquid in gaps is important in practical applications such as recovery of oil in rocks using water, flow of lubricants, etc. In all these applications, it is desired to know the depth of penetration of the liquid as a function of pressure at the inlet of the slit, contact angle of the liquid with the solid, surface tension of the liquid/vapor interface and the flexibility of the solid if the solid is deformable. This paper discusses this application of dynamic wetting on flexible solids, which gives the comparison of length of penetration of flexible solid versus rigid solid. This study gives the measure of robustness of the finite element formulation and the mesh motion scheme developed in [13] since in capillary impregnation, contact line is extremely sensitive to the changes in the parameters such as pressure, contact angle and capillary number. The contact line moves much farther leading to larger distortions in the mesh close to the contact line than the case of upstream end of slot coater [13], where one end of free surface is pinned. This study also helps in understanding the physics of capillary impregnation of liquid in flexible slit.

The objectives of this paper are to present the underlying physics for penetration of liquid in a rigid and flexible slit involving the contact line motion, compare the length of penetration for rigid and flexible slit and study the effect of contact angle, pressure, and capillary number on the contact line motion for a flexible solid. Section 2 discusses the model formulation and boundary conditions in a moving reference frame. Section 3 presents the Galerkin finite element formulation for solving the model. Section 4 gives the mesh refinement studies followed by the results section.

2. Model formulation

The geometry for modeling capillary impregnation in a flexible slit consists of liquid penetrating the gap between two rectangular elastic solids. The solids are assumed to be rigid on outer boundaries and at the outlet boundary as shown in Fig. 1. At the inlet of the slit, the solid is flexible and hence, deforms under the action of shear forces from the liquid. Due to the symmetry, only half of the geometry is solved.

The equations are framed in a moving reference frame, which moves with the velocity of the penetration of the liquid, $-V_{S,x}$. This changes the transient capillary impregnation problem to a steady-state problem, where the liquid/vapor free surface freely slides along the symmetry plane, the undeformed solid moves with velocity, $V_{S,x}$ and there is no net flow rate of the liquid at the outflow plane as shown in Fig. 1. In this paper, all the equations and boundary conditions both liquid and solid domains are in Eulerian frame of reference.

The liquid/vapor free surface wets the solid as it moves across the solid surface. The solid deforms under the action of surface tensions forces arising at the contact line. The aim of this paper is to take into account the effect of solid deformation to calculate the position of the contact line. In order to calculate the position of the contact line, mass and momentum in solid and liquid domains needs to be conserved and appropriate boundary conditions developed from the physics of the problem should be applied and mesh motion scheme, which can track the dynamic contact line, is needed. The next few sections discuss these aspects.

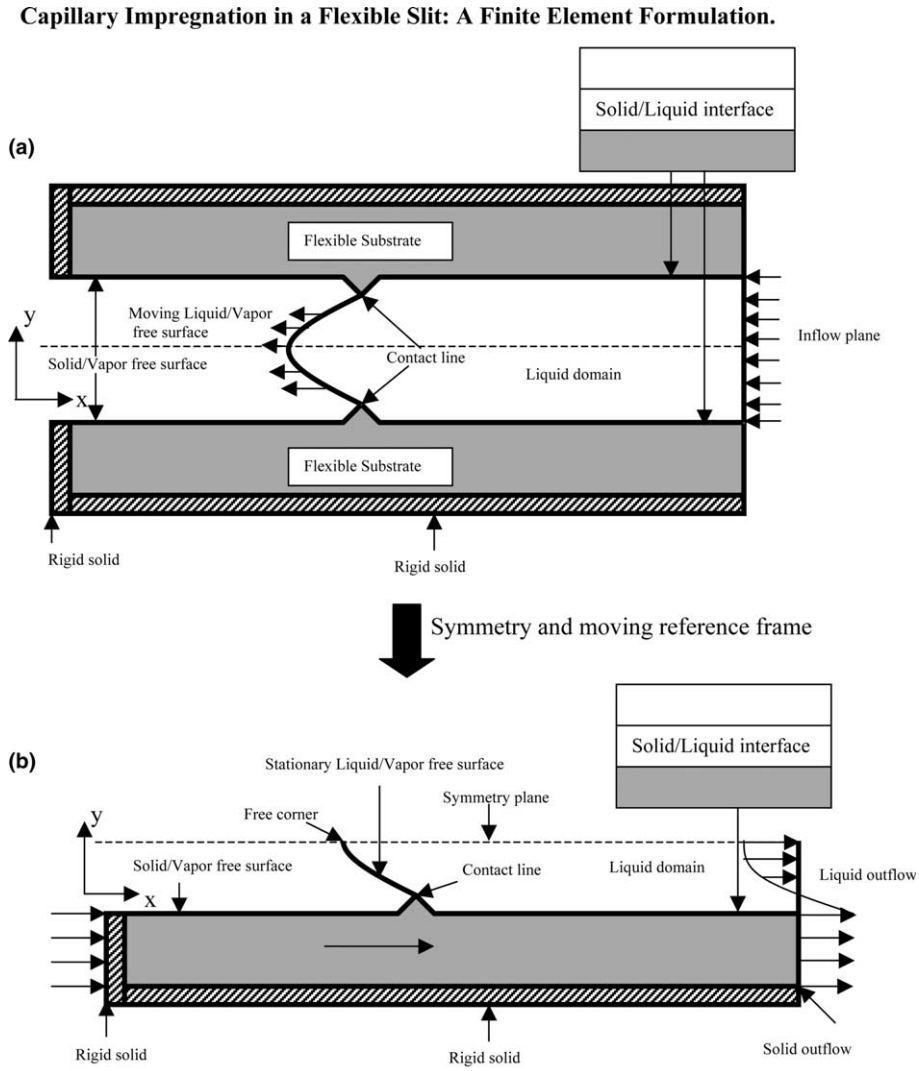

Fig. 1. (a) Capillary impregnation of liquid in a flexible slit and (b) problem solved in a moving reference frame with liquid/vapor free surface free to slide on symmetry plane.

2.1. Conservation of mass and momentum in liquid domain

Flow is assumed to be laminar, two-dimensional, and incompressible. The motion of liquid/vapor meniscus in the flexible slit is considered to be steady and hence, velocity of penetration is constant. In the liquid domain, Stokes and continuity equations are solved to balance momentum and mass, respectively. Stokes equation (2) in dimensionless form given in [13] at zero Reynolds number, negligible body forces such as gravity and for Newtonian liquids is

$$\nabla \cdot \mathbf{T}_{\mathrm{L}} = 0, \tag{2}$$

where

$$\mathbf{T}_{\mathrm{L}} = \left(-p_{\mathrm{L}}\mathbf{I} + \left(\nabla\mathbf{v}_{\mathrm{L}} + \nabla\mathbf{v}_{\mathrm{L}}^{\mathrm{T}}\right)\right), \tag{3}$$

$\mathbf{T}_{\mathrm{L}}$ is the stress tensor, p_{L} is the dimensionless pressure which is equal to $p'_{\mathrm{L}}L/\mu U_{\mathrm{L}}$, $\mathbf{v}_{\mathrm{L}}$ is the velocity vector, L is the characteristic length scale, which is chosen to be the half width of the slit, U_{L} is the characteristic speed which is chosen to be as the speed of the undeformed solid, μ is the viscosity of the liquid, p'_{L} is the dimensional pressure, and $\underline{\underline{\mathbf{I}}}$ is the identity tensor.

Conservation of mass for an incompressible fluid is given by the continuity equation:

$$\nabla \cdot \mathbf{v}_{\mathrm{L}} = 0. \tag{4}$$

2.2. Conservation of mass and momentum in solid domain

In the solid domain, Cauchy's equation of equilibrium, with negligible inertia and body forces, is solved to conserve momentum. Solids such as rubber which are normally incompressible are considered in the model and hence, incompressibility constraint is solved to solve for pressure in the solid. The equations to be solved in the solid domain in dimensionless form are given in [14].

$$\nabla \cdot \mathbf{T}_{\mathrm{S}} = 0, \tag{5}$$

where

$$\mathbf{T}_{\mathrm{S}} = ((-p_{\mathrm{S}} - 2fG + G)\mathbf{I} + f\mathbf{B} - (1-f)\mathbf{B}^{-1}), \tag{6}$$

where the solid stress, $\mathbf{T}_{\mathrm{S}}$, is predicted by Mooney–Rivlin constitutive law [15] for incompressible, rubber-like solids, $p_{\mathrm{S}} = p'_{\mathrm{S}}L^2/Gu^2$, p_{S} is the dimensionless pressure in the solid, p'_{S} is the dimensional pressure in the solid, f is a material constant which varies between 0 and 1, and $\mathbf{B} = \mathbf{F}\mathbf{F}^{\mathrm{T}}$ is the left Cauchy–Green deformation tensor. $\mathbf{F}$ is the deformation gradient tensor in the deformed coordinates.

The incompressibility constraint sets the determinant of the deformation gradient tensor to be 1 as seen in the following equation:

$$|\mathbf{F}| = 1. \tag{7}$$

Section 2.3 discusses the boundary conditions applied on the solid and liquid domains.

2.3. Boundary conditions

Fig. 1 shows the boundary conditions applied on the solid and liquid domains in a moving reference frame. Boundary conditions are applied to solve the velocity, pressure fields in liquid domain and displacement, pressure fields in solid domain.

2.3.1. Boundary conditions on liquid domain

In a moving frame of reference, the pressure gradient forces needs to balance the Couette forces from the shear flow in the entire liquid domain for the net flow rate to be zero. At steady state and in a moving frame of reference, the liquid/vapor free surface is stationary but it changes its location such that net flow rate is zero.

Along the liquid/vapor interface, a normal stress balance condition is applied on the liquid velocity equations

$$-\vec{\mathbf{n}} \cdot \mathbf{T}_{\mathrm{L}} = \vec{\mathbf{n}} \cdot p_{\mathrm{ext}}\mathbf{I} + \frac{2H\vec{\mathbf{n}}}{Ca}, \tag{8}$$

where H is the surface mean curvature, $Ca = \mu V_{S,x}/\sigma_{LV}$ is the capillary number, σ_{LV} is the solid/liquid surface tension. The capillary number scales the significance of the viscous forces to that of the surface tension forces at the liquid/vapor free surface.

At the inlet of the liquid domain, pressure is specified as the inflow boundary condition. Along the solid/liquid interface, over two elements, the *Navier slip condition* is applied to the tangential equation to relieve the stress singularity in the liquid is relieved.

$$\frac{1}{\beta}(\mathbf{v}_L - \mathbf{v}_S) = \vec{\mathbf{n}} \cdot \mathbf{T}_L, \tag{9}$$

where β is the slip coefficient. $\beta = 0$ corresponds to no slip condition, whereas $\beta = \infty$ corresponds to free slip condition. The no penetration condition is applied to the normal equation of the momentum, as the liquid does not penetrate the solid.

$$\vec{\mathbf{n}} \cdot \mathbf{v}_L = 0. \tag{10}$$

Away from the contact node (further than 2 elements), the no slip condition is applied and the velocity of the liquid is equal to velocity of solid.

The vertical velocity is set to zero along the symmetry plane and the since the shear stress is zero, Eq. (11) is applied on the x-liquid momentum equation

$$\vec{\mathbf{n}} \cdot \mathbf{T}_L = 0. \tag{11}$$

2.3.2. Boundary conditions on solid domain

At the solid outflow end, the solid displacement is calculated using Cauchy's equation of equilibrium and fully developed velocity profile. Using the no slip boundary condition condition, i.e., $v_{L,x} = V_{S,x}$ at $y = h_S$ and $T_{L,xy} = 0$ at $y = h_S + h_L$, the velocity profile in dimensional form is as follows:

$$v_{L,x} = V_{S,x}\left[1 + 1.5\left(\frac{y - h_S}{h_L}\right)^2 - 3\left(\frac{y - h_S}{h_L}\right)\right]. \tag{12}$$

The solid displacement is calculated with $T_{s,xx} = -p$ and $T_{s,xy} = G(\mathrm{d}u/\mathrm{d}y)$, using Cauchy's equation of equilibrium and boundary conditions $u = 0$ at $y = 0$ and $T_{S,xy} = -3\mu V_{S,x}/h_L$, which can be derived from the Couette–Poiseuille flow velocity profile Eq. (12) at $y = h_S$

$$u = \left(\frac{1.5\mu V_{S,x}}{Gh_L^2}\right)y^2 - \left[\left(\frac{3\mu V_{S,x}h_S}{Gh_L^2}\right) + \left(\frac{3\mu V_{S,x}}{Gh_L}\right)\right]y = 1.5E_S y^2 - \left(3E_S\frac{h_S}{h_L} + 3E_S\right)y, \tag{13}$$

where u is the displacement in the x-direction, V is the displacement in the y-direction, h_S is the height of solid, h_L is the liquid film thickness, y is the dimensional position in the y-direction, G is the shear modulus and $E_S = (\mu V_{S,x}/GL)$ = (Viscous forces/Elastic forces). The elasticity number scales the significance of the viscous forces along the solid/liquid interface to that of the elastic forces in the solid.

Along the solid/vapor and solid/liquid interfaces, normal stress balance condition is used on the displacement of the solid.

Solid/vapor interface

$$-\vec{\mathbf{n}} \cdot \mathbf{T}_S = \vec{\mathbf{n}} \cdot p_{ext}\mathbf{I} + \frac{2H\vec{\mathbf{n}}}{Ca_{ESV}}; \quad Ca_{ESV} = \frac{GL}{\sigma_{SV}}. \tag{14a}$$

Solid/liquid interface

$$-\vec{\mathbf{n}} \cdot \mathbf{T}_S = \vec{\mathbf{n}} \cdot \mathbf{T}_L E_S + \frac{2H\vec{\mathbf{n}}}{Ca_{ESL}}; \quad Ca_{ESL} = \frac{GL}{\sigma_{SL}} \tag{14b}$$

where H is the surface mean curvature, Ca_{ESV} is the elastic capillary number for solid/vapor interface, Ca_{ESL} is the elastic capillary number for solid/liquid interface, σ_{SV} is the solid/vapor surface tension and σ_{SL} is the solid/liquid surface tension. Elastic capillary number scales the elastic forces in the solid to the surface tension forces along the solid/vapor interface or solid/liquid interface.

Along the rigid solid boundaries, zero displacement boundary condition is applied.

2.3.3. Boundary conditions at the contact line

The recipe for the boundary conditions applied at the dynamic contact line is obtained from [13]. Singularity in elastic stress [14] results at the contact line due to line force acting from the liquid/vapor surface tension, which results in an infinite displacement as given in [16]. The singularity in the solid is relieved by distributing the line force over a finite contact region. Similarly, singularity in viscous stress in liquid domain results at the contact line due to the double-valued velocity and is relieved by Navier slip condition. Following boundary conditions are applied at the contact line:

- x-component of fluid momentum residual is replaced by kinematic condition – $V_{L,x} = 0$,
- y-component of fluid momentum residual is replaced by no penetration – $V_{L,y} = 0$,
- x-component of solid momentum residual is added to capillary condition from solid/liquid, solid/vapor and liquid/vapor free surfaces and normal stress from the liquid,
- y-component of solid momentum residual is added to capillary condition from solid/liquid, solid/vapor and liquid/vapor free surfaces and normal stress from the liquid,
- x-component of mesh displacement is replaced by contact angle condition with respect to the bisecting plane – $\vec{\mathbf{m}}_{LV} \cdot (\vec{\mathbf{m}}_{SL} - \vec{\mathbf{m}}_{SV})/|\vec{\mathbf{m}}_{SL} - \vec{\mathbf{m}}_{SV}| = \cos\theta$.
- y-component of mesh displacement is replaced by – $\mathrm{d}y = v$ (Contact node moves along with the real solid in the vertical direction).

2.4. Mesh motion schemes

ALE method of mesh motion is used for studying dynamic wetting on flexible substrates [13]. Capillary impregnation in a flexible slit is a dynamic wetting problem involving flexible substrate; hence, ALE mesh motion technique is used. In the liquid domain, pseudosolid mesh motion [13,17–20] is implemented and in the solid domain spine method [13] of mesh motion is used. At the free corner, since the liquid/vapor free surface freely slides along the symmetry plane, the kinematic condition gets applied on the x-mesh displacement and since there is zero displacement in the y-direction, y-displacement of the mesh is set to zero. Along the symmetry plane, the y-mesh displacement is set to zero and for x-displacement, nodes are allowed to be shear free so that they can freely slide along the symmetry plane to adjust to the location of the free corner to minimize mesh distortions.

Along the liquid/vapor interface, a kinematic condition is applied on the displacement in the normal direction (x-displacement)

$$\vec{\mathbf{n}} \cdot \mathbf{v}_L = 0. \tag{15}$$

Along the tangential direction (y-displacement), the nodes are allowed to be shear free.

Along the solid/vapor and solid/liquid free surfaces, the vertical motion of the mesh must conform to the solid. Hence the y-displacement of the mesh is set equal to the y-displacement of the solid:

$$\mathrm{d}y = v. \tag{16}$$

For the x-displacement, the nodes are allowed to be shear free so that they can freely slide and their motion will become independent of the underlying solid. Along the rigid solid, solid outflow and liquid inflow boundaries, zero mesh displacement boundary condition is applied.

3. Numerical method

The numerical method used for solving the equations is the Galerkin finite element method [9,10,19,20]. Galerkin finite element method approximates the solution in each element to be the product of the nodal unknowns and the basis functions. The basis functions for velocity and displacement unknowns are chosen to be biquadratic and for the pressure unknowns to be bilinear. The order of basis functions for pressure is chosen to be one order less than that of velocity or displacement in order to satisfy the Ladyzhenskaya–Babuska–Brezzi (LBB) condition [21]. The nodal unknowns in an element for velocity and displacements fields are 9 and for pressure in both solid and liquid domains are 4.

The momentum residual in the liquid domain is integrated by parts using the basis function as weighting function. The weighted residual in the weak form is expressed as follows:

$$R_i^{\mathrm{m}} = \int_V (\nabla \cdot \mathbf{T}_{\mathrm{L}})\phi_i \, \mathrm{d}v = -\int_V (\nabla \phi_i \cdot \mathbf{T}_{\mathrm{L}}) \, \mathrm{d}v + \int_S \phi_i (\vec{\mathbf{n}} \cdot \mathbf{T}_{\mathrm{L}}) \, \mathrm{d}s, \tag{17}$$

where ϕ_i denotes the biquadratic basis function.

The Continuity residual is obtained as follows:

$$R_i^{\mathrm{c}} = \int_V (\nabla \cdot \mathbf{v}_{\mathrm{L}})\psi_i \, \mathrm{d}v, \tag{18}$$

where ψ_i is the bilinear basis function.

The momentum residual in the solid domain is obtained as follows:

$$R_i^{\mathrm{m}} = \int_V (\nabla \cdot \mathbf{T}_{\mathrm{S}})\phi_i \, \mathrm{d}v = -\int_V (\nabla \phi_i \cdot \mathbf{T}_{\mathrm{S}}) \, \mathrm{d}v + \int_S \phi_i (\vec{\mathbf{n}} \cdot \mathbf{T}_{\mathrm{S}}) \, \mathrm{d}s. \tag{19}$$

The incompressibility residual in deformed co-ordinates is obtained as follows:

$$R_i^{\mathrm{c}} = \int_V \left(\left| \underline{\underline{\mathbf{I}}} - \nabla \mathbf{u} \right| - 1 \right) \psi_i \, \mathrm{d}v, \tag{20}$$

where $\mathbf{u}$ is the displacement of the solid.

The second term in the momentum residual is a boundary condition term. For the capillary condition, the boundary integral term can be expressed in terms of surface divergence [19] and can be added to the residual. The details of this derivation are provided in [19]. The momentum balance at the contact node, application of boundary conditions and the method of solving residual equations are given in [13].

Section 4 discusses the mesh convergence with change in elements followed by results obtained from the study of effect of downstream pressure, contact angle, capillary number, and elasticity number on dynamic contact line motion. The length of penetration in a rigid slit versus flexible slit is compared.

4. Tests of mesh performance

4.1. Mesh convergence

The first step in this analysis is to perform convergence tests to determine the optimum number of elements in x and y directions. The elements are stretched more towards the contact node by the stretching function given in Eq. (21)

$$\Delta x_1 = L\left(\frac{1-\eta}{1-\eta^{ne}}\right), \quad \Delta x_2 = \eta \Delta x_1, \quad \Delta x_3 = \eta \Delta x_2, \ldots, \Delta x_{ne} = \eta \Delta x_{ne-1}, \tag{21}$$

where Δx_1 is the size of the first element, Δx_2 is the size of the second element and so on, L is the total length of the domain over which stretching is applied, ne is the number of elements in the domain, and η is the stretching parameter. For $\eta > 1$, the elements sizes increase over the domain. Stretching enables to concentrate more number of elements near the contact line where it is important to capture the physics accurately and less number of elements away from the contact line and hence, helps in reducing the total number of elements required for convergence.

Here, convergence means with further refinement, the change in the shapes of the solid and liquid/vapor free surfaces is negligible and change in the x-position of the contact node is small (order of 10^{-2}). First, the number of elements in y-direction is kept constant at 8 elements in both solid and liquid domains, and the number of elements in x-direction are increased to obtain the base case mesh such that the size of the element adjacent to the element near the contact node by 50% when compared to the coarse mesh. Then the base case mesh is further refined by decreasing the element size adjacent to the element at the contact node to refined mesh as shown in Table 1. The tests were performed for a base case of pressure of 29, capillary number of 0.02, elasticity number of 0.001, contact angle of 90°, and elastic capillary number 10. Navier slip coefficient $\beta = 0.00001$, slip length over 2 elements, and contact region $L_{CR} = 0.1$ [13] are used for the simulations.

The solid-free surface, liquid/vapor free surfaces, contours of pressure are compared to show convergence in Figs. 2 and 3. The elements adjacent to the contact node are fixed and hence, their sizes do not change with refinement. There is a change in the order of 10^{-2} for the dynamic contact line position. Fig. 2 shows the comparison of liquid/vapor free surfaces and solid-free surfaces. It is observed that there is negligible change in the solid free surface and the shape of the liquid/vapor free surface remains the same except that dynamic contact line got shifted in the x-direction approximately by 0.0198 from the base case to refined mesh. Fig. 2(a) shows that the dip in the solid-free surface is due to the incompressibility constraint. The displacement approaches to zero at distances far away from the contact line. Maximum displacement is observed at the contact line.

Fig. 3 shows the comparison of contours for pressure fields for base case versus refined mesh. It can be seen that the pressure field vary linearly at far away from the contact line and the pressure contours match there. Close to the contact line, there is small deviation in the contour shapes. After optimizing the elements in x-direction and comparing the free surfaces and contours it has been concluded that 26 elements with $\eta = 1.1$ on the solid/liquid side, 12 elements with $\eta = 0.77$ on the solid/vapor side are sufficient to get a converged solution with respect to elements in x-direction.

Next, the number of elements in x-direction is kept constant in both solid and liquid domains, and the number of elements in y-direction is increased to obtain the base case mesh such that the size of the element decreases by 50% when compared to the coarse mesh. Then the base case mesh is further refined by decreasing the element size adjacent to the element at the contact node to refined mesh as shown in Table 2. Computations are performed at the same parameter values used for determining the number of elements in x-direction.

Table 1
Convergence test for mesh refinement, with different number of elements in x-direction

	Number of elements ($x \times y$)	Size of the smallest element ($\Delta x \times \Delta y$)	x-position of contact line
Coarse mesh	$20 \times 9 \times 8 \times 8$	0.173967×0.125	9.02993
Base case	$26 \times 12 \times 8 \times 8$	0.090496×0.125	8.99585
Refined mesh	$30 \times 15 \times 8 \times 8$	0.05988×0.125	8.97596

The reported element size is that of the element adjacent to the element at the contact line on the solid/liquid interface.
Parameters pressure = 29, $\theta = 90°$, $E_S = 0.001$ and $Ca_{ESV} = Ca_{ESL} = 10$ are used.

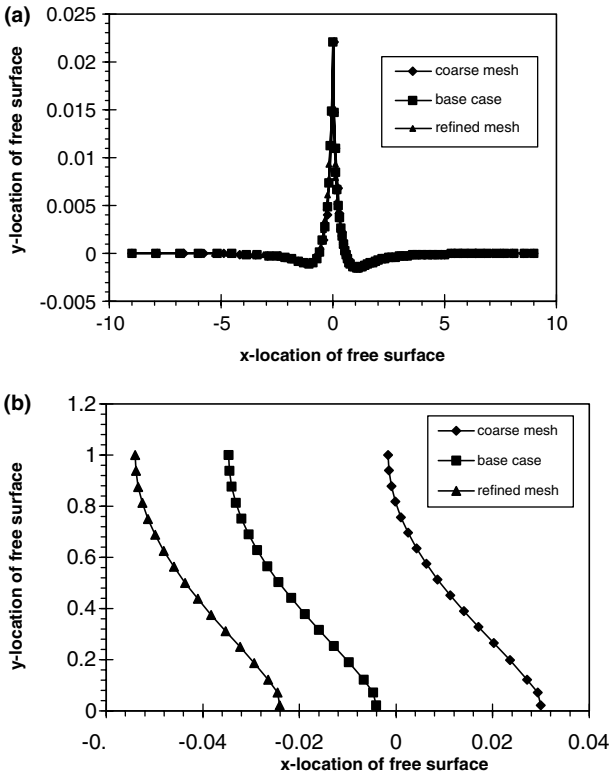

Fig. 2. Comparison of (a) free surface of solid; (b) free surface of the liquid for three different levels of mesh refinement in x-direction. The contact angle of 90°, $Ca_{ESV} = Ca_{ESL} = 10$, $Ca = 0.02$, $E_S = 0.001$, pressure = 29 are used for this comparison.

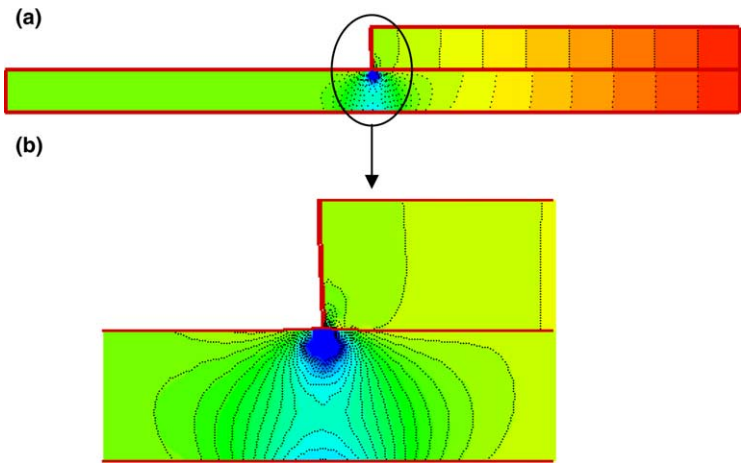

Fig. 3. Comparison of contour plot of pressure field (a) for full domain (b) close to the contact line with base case (solid) versus refined mesh (dash) for mesh refinement in x-direction. The contact angle of 90°, $Ca_{ESV} = Ca_{ESL} = 10$, $E_S = 0.001$, $Ca = 0.02$ and pressure = 29 are used for this comparison. The minimum pressure contour level was set at -50, maximum pressure contour level was set at 29 and the number of levels was set to 26.

Table 2
Convergence test for mesh refinement, with different number of elements in y-direction

	Number of elements ($x \times y$)	Size of the smallest element ($\Delta x \times \Delta y$)	x-position of contact line
Coarse mesh	$20 \times 9 \times 4 \times 4$	0.173967×0.25	9.15834
Base case	$20 \times 9 \times 8 \times 8$	0.173967×0.125	9.02993
Refined mesh	$20 \times 9 \times 12 \times 12$	0.173967×0.0833	9.00332

The same parameters and notations were used as in Table 1.

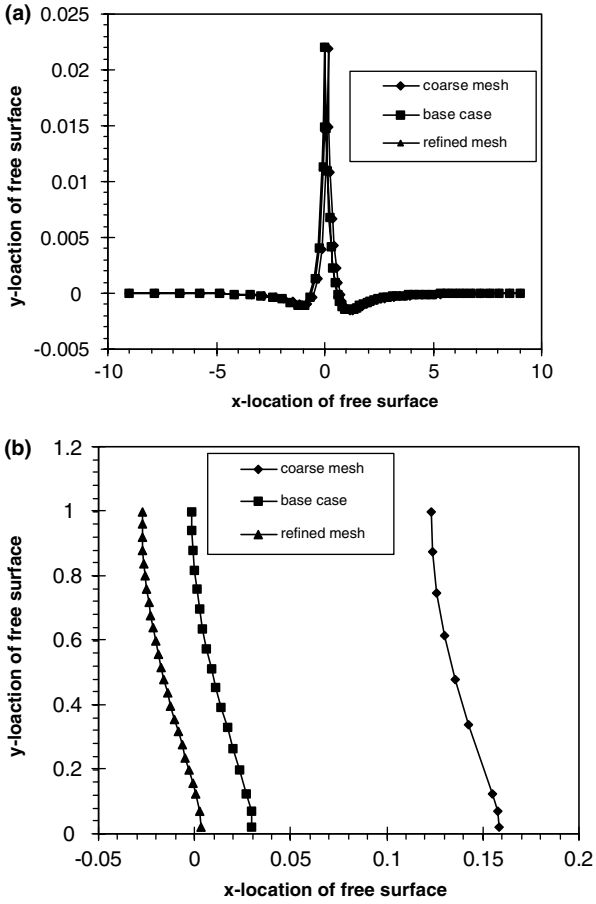

Fig. 4. Comparison of (a) free surface of solid; (b) free surface of the liquid for three different levels of mesh refinement in y-direction. The contact angle of 90°, $Ca_{ESV} = Ca_{ESL} = 10$, $Ca = 0.02$, $E_S = 0.001$, pressure = 29 are used for this comparison.

The solid-free surface, liquid/vapor free surfaces, contours of pressure are compared to show convergence in Figs. 4 and 5. The elements adjacent to the contact node are fixed and hence, their sizes do not change with refinement. There is a change in the order of 10^{-2} for the dynamic contact line position. Fig. 4 shows the comparison of liquid/vapor free surfaces and solid free surfaces. It is observed that there is negligible change in the solid-free surface and the shape of the liquid/vapor free surface remains the same except that dynamic contact line got shifted in the x-direction approximately by 0.026 from the base case to refined mesh.

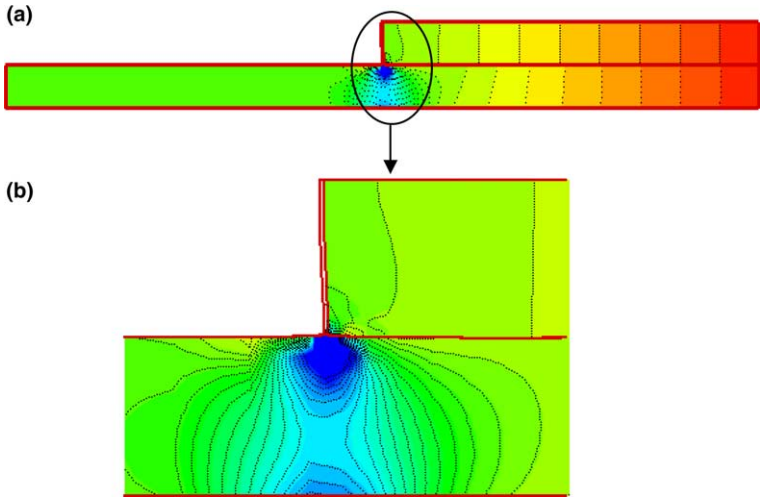

Fig. 5. Comparison of contour plot of pressure field (a) for full domain (b) close to the contact line with base case (solid) versus refined mesh (dash) for mesh refinement in y-direction. The contact angle of 90°, $Ca_{ESV} = Ca_{ESL} = 10$, $E_S = 0.001$, $Ca = 0.02$ and pressure = 29 are used for this comparison. The minimum pressure contour level was set at -50, maximum pressure contour level was set at 29 and the number of levels was set to 26.

Fig. 5 shows the comparison of contours for pressure fields for base case versus refined mesh. Close to the contact line, there is small deviation in the contour shapes. After optimizing the elements in y-direction and comparing the free surfaces and contours it has been concluded that 8 elements in the liquid domain, 8 elements in the solid domain are sufficient to get a converged solution with respect to elements in y-direction. Hence, from the mesh refinement studies it can concluded that 26 elements with $\eta = 1.1$ on the solid/liquid side, 12 elements with $\eta = 0.77$ on the solid/vapor side, 8 elements in the liquid domain and 8 elements in the solid domain are required for performing parametric studies.

5. Results and discussion

5.1. Base case for wetting on a flexible substrate

Figs. 6–8 display contour plots of pressure, velocity, and displacement fields for pressure of 29, capillary number of 0.02, elasticity number of 0.001, contact angle of 90°, and elastic capillary number of 10.

Fig. 6 shows the contours of pressure fields in the solid and liquid domains near the contact line. The pressure contours for the solid and liquid domain match at the downstream end, as there is negligible displacement in the vertical direction even though the solid is sheared there. Hence, the pressure in the solid is equal to the pressure in the liquid near the outflow plane and both vary linearly consistent with fully developed flow. Near the contact node, there is a low-pressure region in both the solid and liquid phases. The pressure in the solid near the contact node is less than that of the liquid because the solid is in tension there due to the action of liquid/vapor surface tension pulling upward at dynamic contact line. The pressure variation is one-dimensional (along the x-direction) towards the outflow

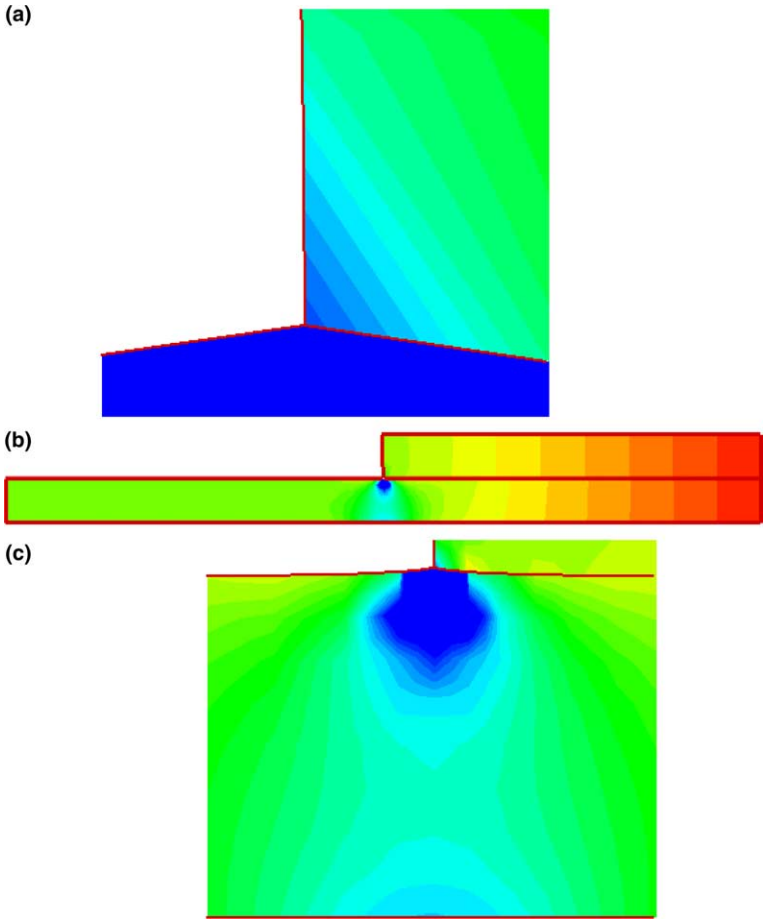

Fig. 6. Contour plots of pressure field (a) liquid domain close to the contact line; (b) full domain; and (c) solid domain close to the contact line with contact angle of 90°, $Ca_{ESV} = Ca_{ESL} = 10$, $E_S = 0.001$, $Ca = 0.02$ and pressure = 29. The minimum pressure contour level was set at −50, maximum pressure contour level was set at 29 and the number of levels was set to 26.

plane. Close to the free surface near the dynamic contact line, liquid turns around and hence pressure variation is two-dimensional there. Fig. 9 shows that the pressure in the solid and liquid goes through a minimum at the contact line and then increases to the downstream almost linearly for most of the domain along the solid/liquid interface. Close to the contact line, pressure in the solid deviates from linear variation. The pressure variation in solid and liquid domains follows the same trend as that of upstream end of slot coater.

Fig. 7 shows the contours of horizontal velocity field in the liquid domain and vertical displacement field in the solid domain near the contact line. The horizontal velocity is zero at the contact node and rises to web velocity through the Navier slip condition (Eq. (9)) over the slip length. After the slip length, the velocity of the liquid is equal to that of the solid because of the no slip condition. The horizontal velocity is one-dimensional on the symmetry line and then the liquid turn around near the meniscus where the flow is two-dimensional and then the horizontal velocity becomes fully developed flow close to the outflow plane such that the net flow rate is zero.

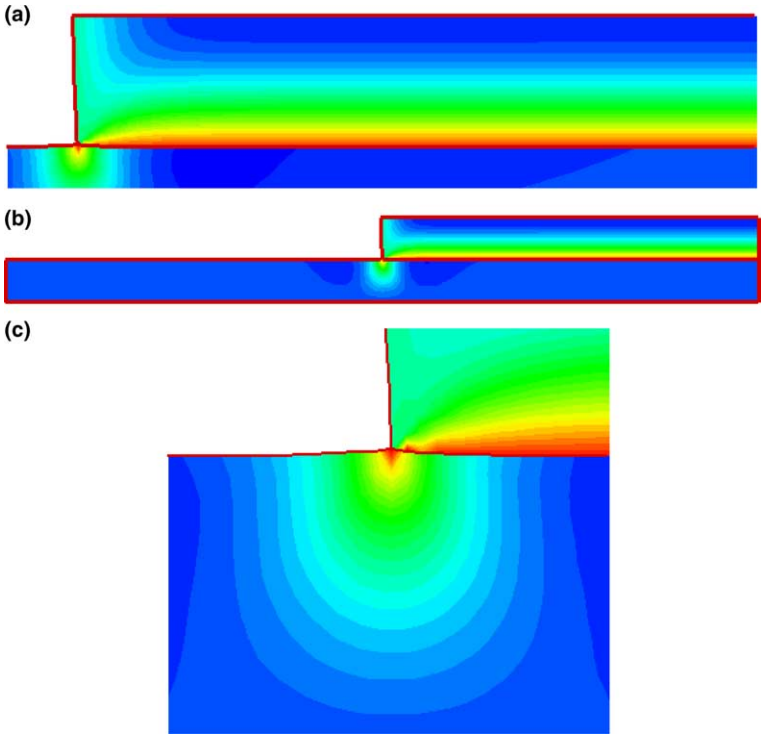

Fig. 7. Contour plots of (a) horizontal velocity field close to the contact line; (b) full domain; and (c) vertical displacement field close to the contact line with contact angle of 90°, $Ca_{ESV} = Ca_{ESL} = 10$, $E_S = 0.001$, $Ca = 0.02$ and pressure = 29. The horizontal velocity minimum contour level was set at −0.5 and maximum contour level was set at 1 and the number of levels was set to 26. The vertical displacement minimum contour level was set at −0.001 and maximum contour level was set at 0.021 and the number of levels was set to 26.

A maximum in vertical displacement of the solid occurs at the contact node because of the line force pulling the contact line upwards and reducing the gap size. The downstream end of the liquid domain corresponds to fully developed flow and the vertical displacement is zero.

Fig. 8(a) shows the contours of vertical velocity field in the liquid domain. The vertical velocity in liquid is zero for most of the domain except near the upstream end where the fluid turns around to flow downstream. At the contact node vertical velocity is zero. Fig. 8(c) shows the horizontal displacement field in the solid domain near the contact line. Horizontal displacement field contours show that near the downstream region of the contact node, solid is sheared towards the contact node because of the shear forces from the liquid and line force. Upstream and downstream of the contact node, solid is sheared towards the contact node because of the line force pulling the solid.

Fig. 10 shows the horizontal displacement varying along the substrate thickness where the solid is getting sheared along the solid/liquid interface. At the outflow plane, the horizontal displacement is parabolic as a result of shear forces and pressure forces acting there. Close to the contact line, the solid displacement is zero at the bottom of the solid and the displacement of the solid at the surface is resultant of line force, shear forces from the liquid and the pressure forces.

The displacement at the surface close to the contact line comes out to be higher than that at the outflow plane because of line force. Displacements decay to zero at the inflow plane of the solid. In general, pres-

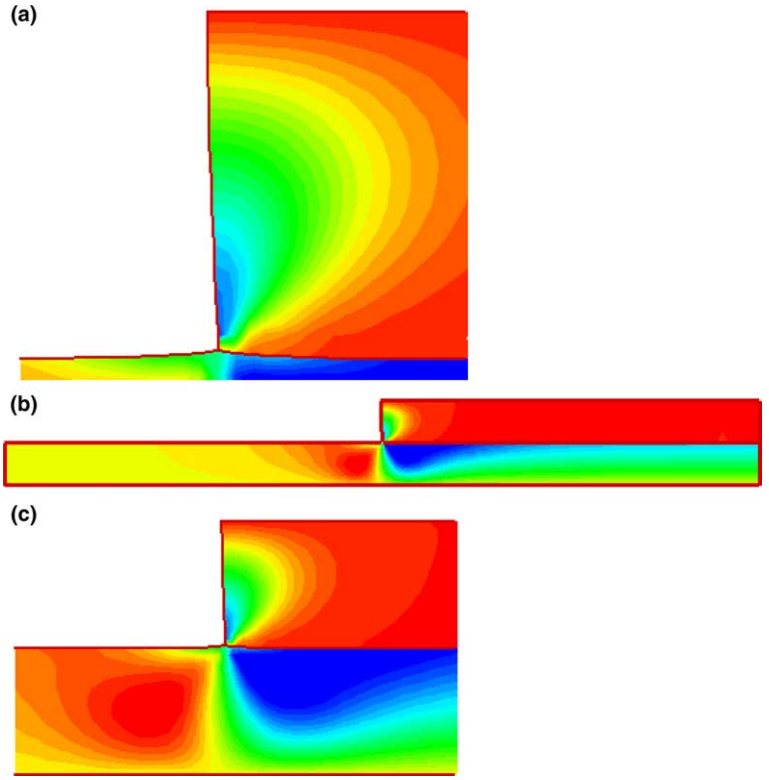

Fig. 8. Contour plots of (a) vertical velocity field close to the contact line; (b) full domain; and (c) horizontal displacement field close to the contact line with contact angle of 90°, $Ca_{ESV} = Ca_{ESL} = 10$, $E_S = 0.001$, $Ca = 0.02$ and pressure = 29. The vertical velocity minimum contour level was set at -0.68 and maximum contour level was set at 0 and the number of levels was set to 26. The horizontal displacement minimum contour level was set at -0.006 and maximum contour level was set at 0.002 and the number of levels was set to 26.

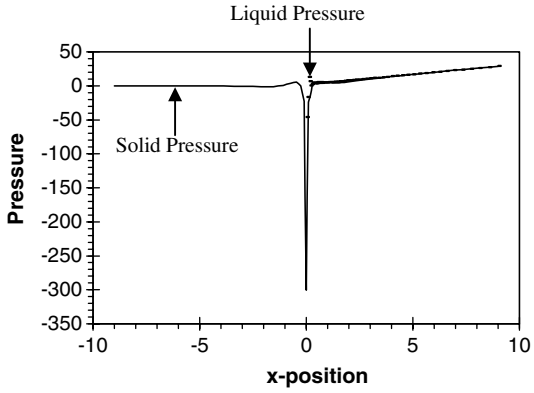

Fig. 9. Variation of pressure in solid and liquid as a function of x-position along the solid surface for pressure = 29, $E_S = 0.001$, contact angle = 90° and $Ca = 0.02$.

sure, displacement and velocity field contours have similar variation as that of the upstream end of slot coater except that in capillary flow in a flexible slit, the meniscus is very sensitive to the parameters, which can be seen from the following sections.

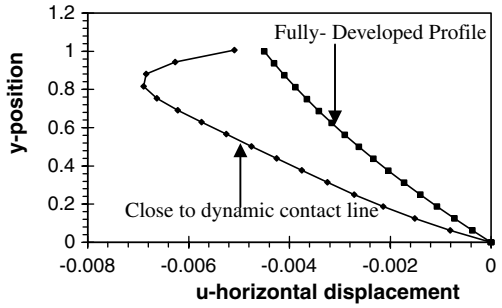

Fig. 10. Line plot of horizontal displacement through the substrate at an arbitrary x-position of 9.236 close to the dynamic contact line for pressure = 29, $Ca = 0.02$, contact angle = 90°, $E_S = 0.001$.

5.2. Analytical model for the dynamic contact line location for rigid solid

To analyze the motion of dynamic contact line, I have derived an analytical model for the location of the dynamic contact line for rigid solid based on Higgins and Scriven [22]. Fig. 11 depicts the domain and geometry of the analytical model. A comparison of the analytical and the finite element models is shown in Fig. 13. The assumptions of the model are that the solid is rigid, the meniscus is an arc of circle and the pressure is a linear function of distance along the substrate.

$$P_{FS} = P_{down} + \left(\frac{\partial P}{\partial x}\right)_{down} (x_{DCL} - x_{down}), \tag{22}$$

where P_{FS} is the pressure at the meniscus, P_{down} is the pressure at the downstream end, $(\partial P/\partial x)_{down}$ is the pressure gradient at the downstream end and is equal to $3\mu v_s/h_L^2$, x_{DCL} is the location of the dynamic contact line and x_{down} is the location of the downstream end.

The liquid pressure at the meniscus comes from the capillary pressure across the curved meniscus:

$$P_{FS} = \frac{\sigma_{LV}}{R}, \tag{23}$$

where R is the radius of curvature. The radius of curvature R is related to the dynamic contact line position by

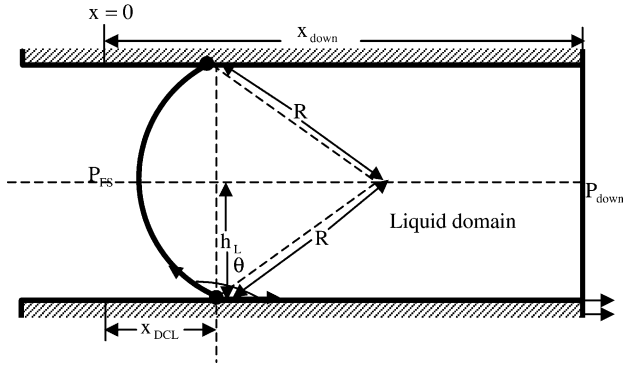

Fig. 11. Schematic of computational domain for analytical model of capillary flow on a rigid substrate moving with a velocity $V_{S,x}$ and liquid/vapor free surface making an angle θ with the solid.

$$R = \frac{-h_L}{\cos\theta}. \tag{24}$$

Eqs. (22)–(24) are combined to develop an equation relating the downstream pressure and the location of dynamic contact line:

$$P_{down} + \frac{3\mu v_S(x_{DCL} - x_{down})}{h_L^2} + \frac{\sigma_{LV}\cos\theta}{h_L} = 0. \tag{25}$$

5.3. Analytical model for the dynamic contact line location for flexible solid

To account for substrate flexibility in the analytical model presented above, vertical displacement of the solid at the contact line modifies the geometric relationship for meniscus curvature (Eq. (24)). As a simple approximation for a flexible solid, the solid at the contact line is assumed to behave as a spring as shown in Fig. 12.

The deformed gap at the contact line is and is assumed to follow Hooke's law:

$$h'_L = h_L\left(1 - \frac{\sigma_{LV}\sin\theta}{G\xi}\right), \tag{26}$$

where ξ is a constant determined from numerical experiments with static wetting such that $\xi = 2.333$. For simplicity, the substrate deformation is assumed only to affect the relationship for curvature and does not affect the pressure profile in the gap. Eqs. (25) and (26) give the following model for the flexible solid:

$$P_{down} + \frac{3\mu v_S(x_{DCL} - x_{down})}{[h_L]^2} + \frac{\sigma_{LV}\cos\theta}{\left[h_L\left(1 - \frac{\sigma_{LV}\sin\theta}{G\xi}\right)\right]} = 0. \tag{27}$$

This equation relates downstream pressure and dynamic contact line position for a flexible solid.

5.4. Study of variation of dynamic contact line with pressure, capillary number, contact angle for rigid, and flexible solids

The dynamic wetting line position variation with different parameters for rigid solid, such as downstream pressure, capillary number and contact angle for rigid solid are presented in Figs. 13–16. The results show

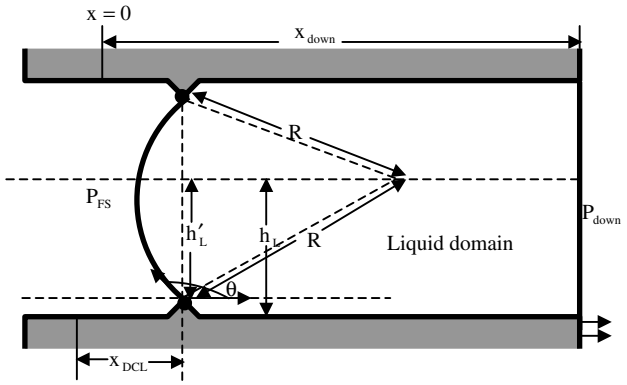

Fig. 12. Schematic of computational domain for analytical model of capillary flow on flexible solid moving with a velocity $V_{S,x}$ and liquid/vapor free surface making an angle θ with the bisecting plane.

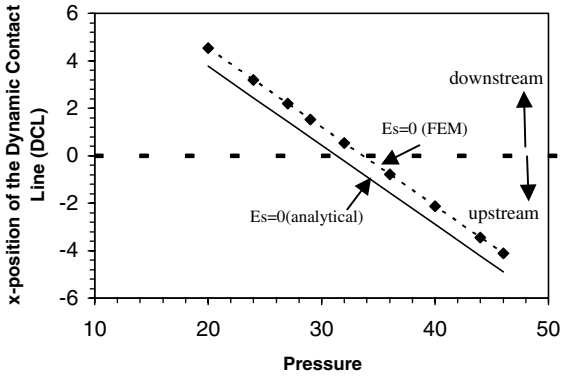

Fig. 13. x-position of the dynamic contact line as a function of pressure at $E_S = 0$, contact angle = 95° and $Ca = 0.02$ for analytical and finite element methods.

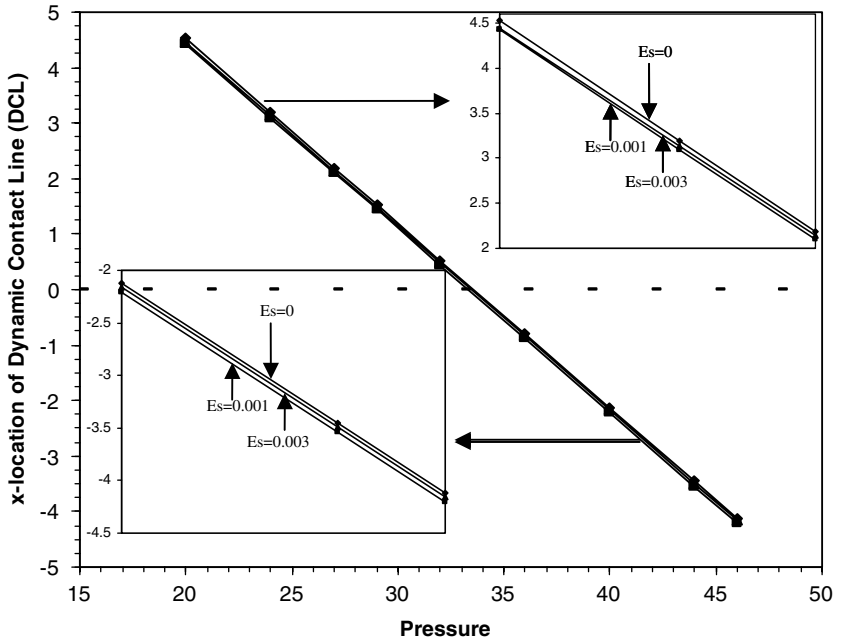

Fig. 14. x-position of the dynamic contact line as a function of pressure for contact angle = 95° and $Ca = 0.02$.

that increase in pressure moves the contact line away from the inflow plane (upstream) increasing the length of penetration, decrease in capillary number pushes the contact line towards the inflow plane (downstream) decreasing the length of penetration if the meniscus is convex from the vapor side, increase in contact angle pushes the contact line towards the inflow plane (downstream) decreasing the length of penetration. Fig. 13 depicts the comparison from analytical and FEM models for the variation of dynamic contact line position with downstream pressure for rigid solid. There is a good qualitative agreement between the analytical and FEM results for rigid solid as shown in Fig. 13. Both the models predict the same trends that increase in pressure moves the contact line away from the inflow plane increasing the length of penetration.

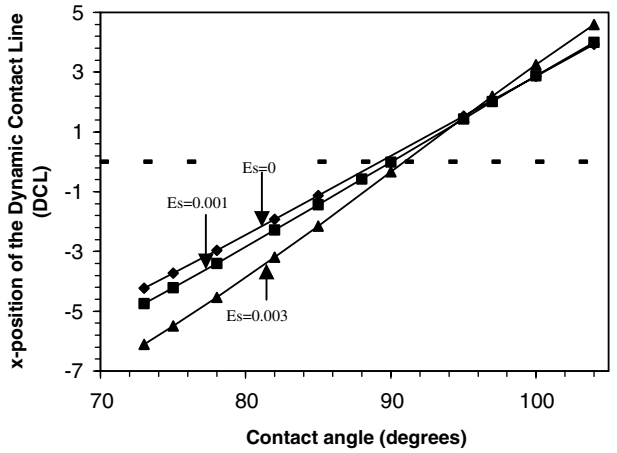

Fig. 15. x-position of the dynamic contact line as a function of contact angle for pressure = 29 and $Ca = 0.02$.

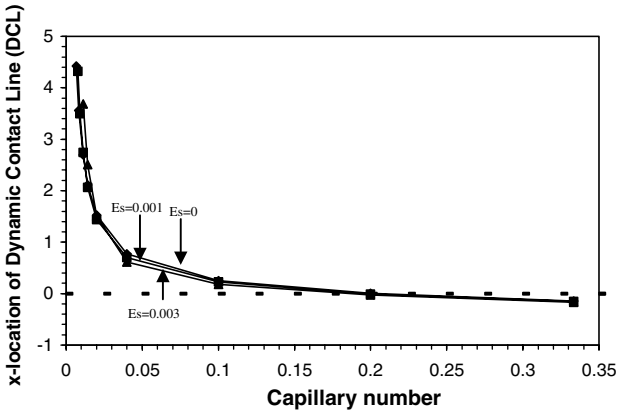

Fig. 16. x-position of the dynamic contact line as a function of capillary number for pressure = 29 and contact angle = 95°.

Fig. 14 shows the variation of dynamic contact line position in FEM model with downstream pressure for a rigid solid. With increase in downstream pressure, with all the other parameters constant, the pressure in the gap goes up. In order to balance the pressure in the liquid and the pressure drop across the meniscus, the meniscus increases the length of the gap pushing the contact node away from the inflow plane (upstream) and similarly when the pressure is decreased; it moves the contact node towards the inflow plane (downstream). The liquid responds to the increase in pressure at the inlet by increasing the length of penetration. This trend is supported qualitatively by Washburn's equation (1) for a rigid pore. If $(P_A + g\rho h)$ in Eq. (1) is maintained constant, it is analogous to the inlet pressure. Then as the inlet pressure is increased, the length of penetration increases for the same time of penetration as seen from Eq. (1).

Fig. 15 shows the variation of dynamic contact line position with contact angle for a rigid solid. With the increase in contact angle, the free surface should decrease the radius of curvature and hence the pressure near the free surface goes up hence, the meniscus decreases the length of penetration in order to balance the pressure and the converse is true when the contact angle is decreased. The analytical model for rigid solid gives a good qualitative agreement for the variation of capillary number and contact angle. Practi-

cally, this result indicates that if two liquids with different contact angles are used to penetrate the slit, the liquid with smaller contact angle penetrates further than the liquid with the higher contact angle for the same time of penetration. This trend of variation of length of penetration with contact angle is supported qualitatively by Washburn's equation (1).

Fig. 16 shows the variation of dynamic contact line position with capillary number for a rigid solid. With decrease in capillary number, all the other parameters constant, surface tension goes up. With increase in surface tension, the pressure drop across the liquid/vapor interface goes up. In order to balance the pressure in the liquid and pressure drop across the meniscus, the length decreases by pushing the contact node towards the inflow plane (downstream). As the surface tension increases, the meniscus shape becomes flat due to the increase in radius of curvature. If two liquids with different surface tensions are allowed to penetrate the slit, the liquid with the higher surface tension penetrates less than the liquid with lower surface tension for the same time of penetration for contact angles greater than 90°. The converse is true for contact angles less than 90°. This trend is supported by Washburn's equation (1).

Fig. 17 depicts the predictions of dynamic contact line location for a flexible solid from the analytical and finite element methods. As the downstream pressure is increased, the contact line moves away from the inflow plane and as the downstream pressure is decreased, the contact line moves towards the inflow plane as shown in Fig. 17. There is good qualitative agreement between the analytical and FEM models. The physics remains the same as that of rigid solid at constant elasticity number. As the downstream pressure is increased, the pressure in the liquid increases and the meniscus balances the pressure drop across the meniscus and the pressure in the liquid by increasing the length of penetration and the converse is true when the pressure is decreased. The quantitative agreement between the analytical and FEM models is not good because of the assumptions of free surface to be an arc of circle and pressure gradient in the liquid domain to be a constant all the way until the meniscus, which is not valid as shown in Fig. 9. Fig. 18 shows the mesh shape near the contact node.

The trends and the physics for the variation of dynamic contact line with capillary number and contact angle at constant elasticity number remain the same as that of rigid solid. The meniscus decreases the length of penetration with decrease in capillary number. Fig. 20 shows the mesh shape near the contact node as the capillary number changes.

The meniscus moves upstream by increasing the length of penetration with decrease in contact angle. The analytical model gives a good qualitative agreement for the variation of capillary number and contact angle at a constant elasticity number. Fig. 21 shows the mesh shape near the contact node as the contact

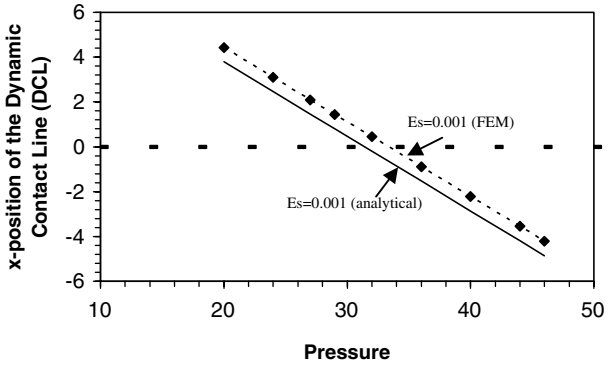

Fig. 17. x-position of the dynamic contact line as a function of pressure at $E_S = 0.001$, contact angle = 95° and $Ca = 0.02$ for analytical and finite element methods.

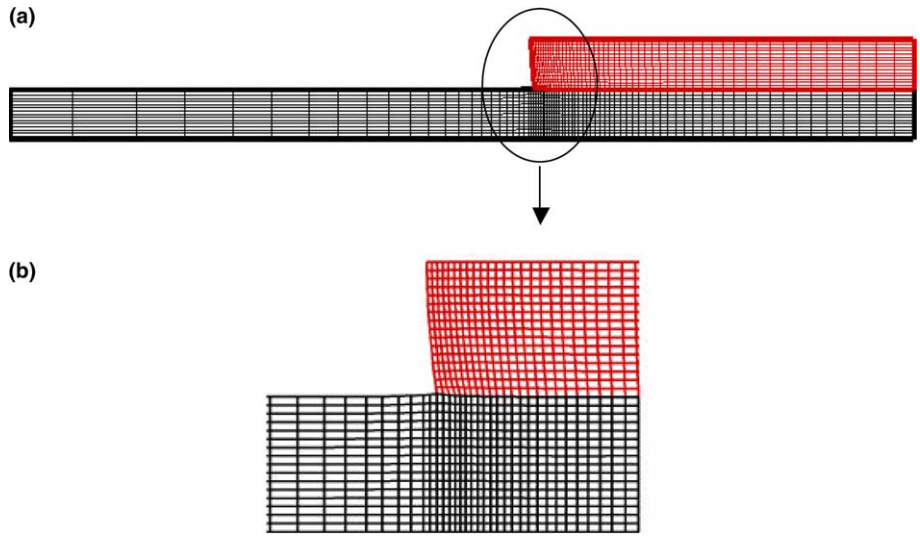

Fig. 18. Shape of the mesh for $E_S = 0.001$, contact angle = 95°, $Ca = 0.02$ and pressure = 29 (a) full domain (b) near the contact node.

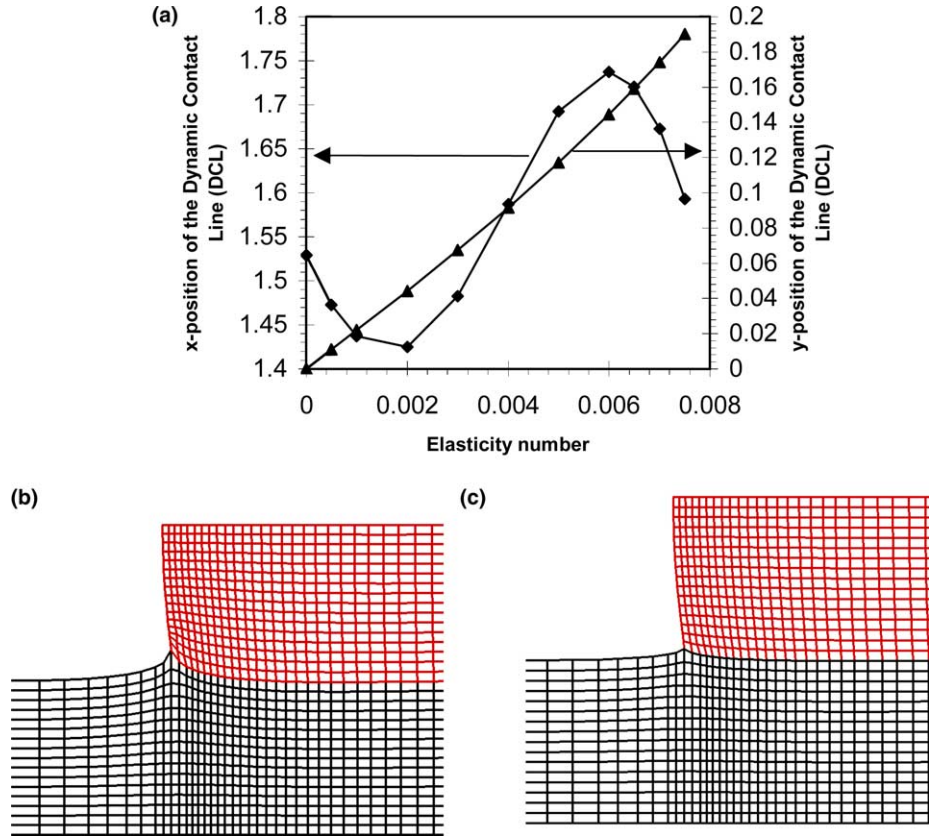

Fig. 19. (a) x-position and y-position of the dynamic contact line as a function of elasticity number for pressure = 29, $Ca = 0.02$ and contact angle = 95° (b) Shape of the mesh near the contact node for $E_S = 0.0075$; (c) Shape of the mesh near the contact node for $E_S = 0.003$.

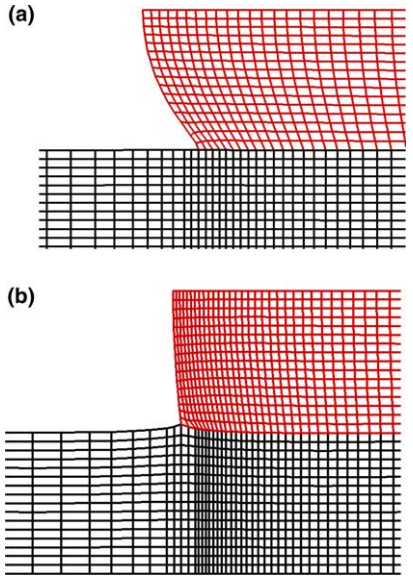

Fig. 20. Shape of the mesh near the contact node for pressure = 29, $E_S = 0.001$, contact angle = 95° (a) $Ca = 0.3333$ and (b) $Ca = 0.0111$.

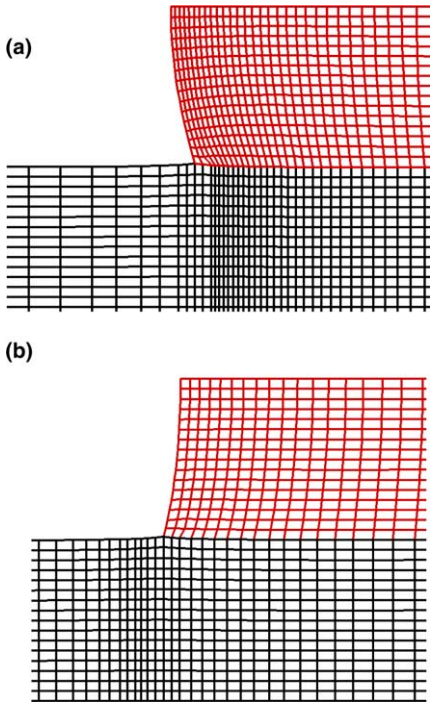

Fig. 21. Shape of the mesh near the contact node for pressure = 29, $E_S = 0.001$, $Ca = 0.02$ (a) contact angle = 104° and (b) contact angle = 73°.

angle changes. The contact line is extremely sensitive to the variation in pressure, capillary number, and contact angle unlike the upstream end of slot coater case [13] for both rigid and flexible solids.

5.5. Effect of substrate stiffness on the position of the dynamic contact line with variation in pressure, capillary number, and contact angle

In general, the variation of the dynamic contact line position with pressure, capillary number and contact angle for constant elasticity number follow the same trends qualitatively as that of rigid solid as discussed in last section. The variation of dynamic contact line position with substrate stiffness for constant pressure, capillary number, and contact angle is discussed in Fig. 19. With increase in flexibility of the solid, the displacement of the contact node increases in the vertical direction as a result of increase in strain as shown in Fig. 19. If the meniscus is concave from the liquid side, the decrease in gap results increase in pressure near the meniscus and hence, the meniscus moves upstream initially, then downstream and then upstream to balance the pressure in the liquid and pressure drop across the meniscus. The analytical model shows that the meniscus moves downstream with increase in elasticity number. The discrepancy is due to the assumption that the pressure varies linearly although way until the meniscus in the analytical model. When the deformations of the solid are small at lower elasticity numbers, the assumptions of the analytical model are reasonable and hence, the trend from the numerical model and analytical model match. But as the elasticity number increases, pressure varies nonlinearly close to the contact line and hence, the trends from the numerical model and analytical models are not same. At high elasticity number, the gap becomes very small and hence, the surface tension forces become very dominant and hence, nonlinearity in pressure is not significant and hence, trends from both the models again match. Fig. 19 show the mesh near the contact node and the location of the contact node variation with elasticity number. With a flexible solid, if the contact line moves upstream then the flexibility of the solid enhances the length of penetration with respect to rigid solid for the same time of penetration, pressure, surface tension, and contact angle. This could be useful in applications, which require faster penetration such as recovery of oil by water. Converse is true for a flexible solid if the contact line moves downstream with respect to rigid solid. This could be useful, where it is desired to have slower penetration such as penetration of coatings in paper pores as faster penetration of coatings could cause non-uniformities in coatings on the paper.

In Fig. 14, the variation of dynamic contact line with substrate flexibility and pressure for finite element method is shown. The contact line moved upstream (away from the inlet) for lower elasticity numbers at constant pressure and then downstream. With a flexible solid, if the contact line moves upstream then the flexibility of the solid enhances the length of penetration with respect to rigid solid for the same time, pressure, surface tension, and contact angle. The meniscus moved always downstream in the analytical model. This could be due to neglecting the stresses from the liquid in the analytical model. As the flexibility of the solid is increased, the pressure near the meniscus increases due to the decrease in the gap and so the meniscus balances the pressure drop across the meniscus and the pressure in the liquid by adjusting the meniscus position. With a flexible solid, the contact line moves upstream with increase in pressure increasing the length of penetration for the same time of penetration, flexibility of the solid, surface tension and contact angle.

Fig. 15 depict the predictions of variation of dynamic contact line position with elasticity number and contact angle. For lower contact angles, the meniscus moves upstream with respect to the rigid solid and for higher contact angles, the meniscus moves downstream with increase in flexibility (at higher elasticity numbers) as shown in Fig. 15. With a flexible solid, if the contact line moves upstream then the flexibility of the solid enhances the length of penetration with respect to rigid solid for the same time, pressure, surface tension, and contact angle. The trends are supported by analytical model at lower contact angles and at higher contact angles only at higher elasticity numbers. The mechanism is similar to the other parameters. With a flexible solid, the contact line moves upstream with decrease in contact angle increasing

the length of penetration for the same time of penetration, flexibility of the solid, surface tension and pressure.

With decrease in capillary number, the line force increases and hence the vertical displacement of the contact node increases which results in the decrease of the gap and hence the pressure near the meniscus in the liquid goes up. If the meniscus is curved concave from the liquid side then the meniscus balances the pressure in the liquid and pressure drop across the meniscus by adjusting the meniscus position. The meniscus moved upstream and away from the gap at higher capillary numbers with increase in elasticity but at lower capillary numbers moved downstream with increase in elasticity number as seen from Fig. 16. The analytical model supports the trend at lower elasticity number. At higher capillary numbers, the trend is not supported by the analytical model due to the negligence of stresses from the liquid. With a flexible solid, the contact line moves upstream with increase in capillary number increasing the length of penetration for the same time of penetration, flexibility of the solid, pressure, and contact angle greater than 90°.

6. Conclusions

This paper presents a finite element formulation for solving capillary impregnation in flexible solids. The equations are framed in a moving reference frame moving with the velocity of the liquid front. The momentum balance, the singularities arising at the dynamic contact line in both solid and liquid domains and the boundary conditions at the contact node are similar to the case of upstream end of slot coater discussed in [13]. The singularity in the solid is relieved by applying the line force over a finite contact region and the singularity in the liquid is relieved by applying the Navier-slip condition.

The parametric studies have shown that the pressure at the outflow, capillary number, contact angle and substrate stiffness affect the motion of the contact line. At constant elasticity numbers, increase in pressure pushes the contact line away from the inlet, increase in capillary number moves the contact node away from the inlet if the meniscus is curved concave from the liquid side; contact angle greater than 90° and increase in contact angle pushes the contact node close to the inlet. The results show that the contact line is very sensitive to these parameters when compared to the case where the liquid/vapor free surface is pinned at one end [13]. The length of penetration increases with increase in inlet pressure, decrease in contact angle and increase in capillary number for contact angle greater than 90° for both rigid and flexible solid with constant elasticity number. These trends match qualitatively with the Washburn's equation (1) for a rigid solid.

The substrate stiffness has an effect on the motion of the contact line. The results have shown that as the substrate stiffness is increased at the same operating parameters, the contact line is pushed away from the gap, then into the gap and then away from the gap. Increase in substrate stiffness decreases the gap width by moving vertically. This paper gives the effect of flexibility on the length of penetration in studying applications such as flow though porous media in recovery of oil in rocks where increasing the flexibility of the solid can enhance the rate of penetration of water and hence, enable to obtain faster recovery of oil. The formulation could also be extended for industrial applications such as flexible roll coating, flexible blade coating, which involve wetting on flexible substrates.

Acknowledgments

I am thankful to Sandia National Laboratories for financial support for this project.

References

[1] S.F. Kistler, P.M. Schweizer, Liquid Film Coating, Chapman & Hall, London, 1997.
[2] J.C. Berg, Wettability, Marcel Dekker, New York, 1993.
[3] E.W. Washburn, The dynamics of capillary flow, Phys. Rev. 17 (1921) 273–283.
[4] R.J. Hansen, T.Y. Toong, Dynamic contact angle and its relationship to forces of hydrodynamic origin, J. Coll. Interf. Sci. 37 (1971) 196–207.
[5] C. Huh, S.G. Mason, The steady movement of a liquid meniscus in a capillary tube, J. Fluid Mech. 81 (1977) 401–419.
[6] L.M. Hocking, A moving fluid interface. Part 2. The removal of the force singularity by a slip flow, J. Fluid Mech. 79 (1977) 209–229.
[7] M.Y. Zhou, P. Sheng, Dynamics of immiscible-fluid displacement in a capillary tube, Phys. Rev. Lett. 64 (1990) 882–885.
[8] W.J. Silliman, L.E. Scriven, Separating flow near a static contact line: slip at a wall and shape of a free surface, J. Comput. Phys. 34 (1980) 287–313.
[9] J. Lowndes, The numerical simulation of the steady movement of a fluid meniscus in a capillary tube, J. Fluid Mech. 101 (1980) 631–646.
[10] J.N. Tilton, The steady movement of an interface between two viscous liquids in a capillary tube, Chem. Eng. Sci. 43 (1988) 1371–1384.
[11] R. Trutschel, U. Schellenberger, Dynamic simulation of free surfaces in capillaries with the finite element method, Int. J. Numer. Methods Fluids 26 (1998) 485–495.
[12] C.A. Powell, M.D. Savage, Numerical simulation of transient free surface flow with moving contact lines, Commun. Numer. Methods Eng. 17 (2001) 581–588.
[13] S. Madasu, R.A. Cairncross, Effect of substrate flexibility on dynamic wetting: A finite element model, Comput. Methods Appl. Mech. Eng. 192 (2003) 2671–2702.
[14] S. Madasu, R.A. Cairncross, Static wetting on flexible substrates: A finite element formulation, Int. J. Numer. Methods Fluids 45 (2004) 301–319.
[15] M.F. Beatty, Topics in finite elasticity: hyperelasticity of rubber, elastomers, and biological tissues – with examples, Appl. Mech. Rev. 40 (1987) 1699–1734.
[16] S. Timeshenko, J.N. Goodier, Theory of Elasticity, McGraw-Hill Book Company, New York, 1951.
[17] P.A. Sackinger, P.R. Schunk, R.R. Rao, A Newton–Raphson pseudo-solid domain mapping technique for free and moving boundary problems: A finite element implementation, J. Comput. Phys. 125 (1996) 83–103.
[18] K.S. Chen, P.R. Schunk, P.A. Sackinger, Finite element analysis of blade and slot coating flows using a Newton–Raphson pseudo solid domain mapping technique and unstructured grids, in: Coating Fundamentals Symposium Proceedings, TAPPI Press, Atlanta, 1995, pp. 131–152.
[19] R.A. Cairncross, P.R. Schunk, T.A. Baer, R.R. Rao, P.A. Sackinger, A finite element method for free surface flows of incompressible fluids in three dimensions. Part I. Boundary fitted mesh motion, Int. J. Numer. Methods Fluids. 33 (2000) 375–403.
[20] T.A. Baer, R.A. Cairncross, P.R. Schunk, R.R. Rao, P.A. Sackinger, A finite element method for free surface flows of incompressible fluids in three dimensions. Part II. Dynamic wetting lines, Int. J. Numer. Methods Fluids. 33 (2000) 405–427.
[21] J.T. Oden, G.F. Carey, Finite Elements, Mathematical Aspects, vol. IV, Prentice-Hall, New Jersey, 1983.
[22] B.G. Higgins, L.E. Scriven, Capillary pressure and viscous pressure drop set bounds on coating bead operability, Chem. Eng. Sci. 35 (1980) 673–682.